JOURNAL OF MATERIALS SCIENCE 24 (1989) 4495–4504

Slip patterns in sliding sphere experiments on (110) single crystal Mn–Zn ferrite

A. BROESE VAN GROENOU, S. E. KADIJK
Philips Research Laboratories, P.O. Box 80000, 5600 JA Eindhoven, The Netherlands

By sliding a 0.25 mm radius ruby sphere on a (1 1 0) Mn–Zn ferrite crystal grooves have been made at speeds from 0.4 to 400 μm sec^{-1}, at loads from 1 to 7 N and after 1 to 100 passes. The temperature was varied from 20 to 290° C. As in indentations, the slip patterns are found on {1 0 0}, {1 1 1} and {1 1 0} slip systems, due to ⟨1 1 0⟩ slip along either a vertical Burgers vector or a vector under 60° with the normal. At low loads the inclined slip systems predominate. Cross-slip in the 60° systems is observed in several directions of sliding. Cross-slip occurs at higher loads on the vertical systems as in indentations. The threshold for both primary and secondary slip is speed dependent. At higher temperatures the main slip system is {1 0 0}, on both vertical and inclined systems. The relative importance of nucleation and propagation of slip is discussed. The groove depth varies with the same parameters as the line patterns, but a direct connection between number of lines and depth could not be made. The angular variation of the depth at low load has been related to the resolved shear stress for the slip systems involved. The result is a yield curve for slip along the inclined Burgers vectors.

1. Introduction

Mn–Zn ferrite crystals are widely used as a material for magnetic recording heads, in both video and data recording. In this application the hard (Vickers hardness 7 GPa) and brittle ($K_{Ic} \simeq 1$ MPa m$^{1/2}$) material is subject to mild wear. The rate of wear depends on the choice of contact plane and the direction of tape motion. Between planes the wear rate of heads against CrO_2 tape varies by a factor 50, while on one plane, (1 1 0), the direction of motion along [1 $\bar{1}$ 0] gives an order of magnitude higher wear than along [0 0 1] [1]. The Knoop hardness along [1 $\bar{1}$ 0] is 10% lower than along [0 0 1] [2, 3]. Anisotropy in mild wear should be related to plastic deformation, but for these magnetic oxides with the spinel structure the mechanical behaviour "is not known well" [4]. From creep experiments above 900° C, slip systems have been derived, all with Burgers vectors along ⟨1 1 0⟩. Slips on {1 0 0} [5], {1 1 1} [4–6] on {1 1 0} [5, 6] were found. From Knoop indentations at room temperature Ito deduced that {1 1 1} and {1 1 0} are important [2].

Recently, sphere indentation experiments were used to study the deformation of a magnetic spinel, $Mn_{0.62}Zn_{0.32}Fe_{2.06}O_4$. By using a ruby sphere of 0.25 mm diameter the indentations showed a variety of slip patterns at low loads [7, 8]. The stress underneath a loaded sphere is known [9, 10], and, as long as the plastic deformation is small, the resolved shear stress (RSS) may be calculated, as for slip on {1 1 0} in MgO [11, 12]. For a spinel, with slip on {1 0 0}, {1 1 1} and {1 1 0}, RSS could be calculated for slip directions along ⟨1 1 0⟩. The elastic approximation allowed the position of the slip lines on the surface to be predicted. A complete analysis of the polygon patterns made by indenting was possible and numerical data on the RSS for primary and secondary slip could be given [7, 8].

The indentation experiments have been extended recently to sliding. With the same equipment as used previously [7, 8, 13, 14], sliding sphere experiments were done on a number of crystal planes. The groove depth varied with load, number of passes, direction and speed of sliding. Above a certain threshold a simple empirical relation is found between depth and load, log (speed) and log (passes) at 20° C. The threshold is lowest for sliding on (1 1 1) and highest on (1 0 0). The effects of more passes or a lower speed of sliding are larger on (1 1 0) than on (1 0 0) or (1 1 1). For the (1 1 0) crystal the temperature was varied from 20 to 290° C, showing a larger influence of load on depth, but without an extra speed effect. This result means that thermal propagation of slip is not the bottleneck in plastic deformation here.

In the indentations on (1 1 0) two patterns of slip lines were distinguished [7], an outer pattern in the form of an octogon, due to vertical slip, and an inner rectangular pattern, due to Burgers vectors along 60° with the surface (Figs 1a to c). In the following the systems will be distinguished by an index, 0 or 60, depending on the direction of the Burgers vector with respect to the normal on the surface. The RSS values used in this paper are taken from a Table in [7].

The outer pattern is caused by vertical slip on three systems, {1 1 1}⟨1 1 0⟩, {0 0 1}⟨1 1 0⟩ and {1 1 0}⟨1 1 0⟩. The lines are coupled and form an octogon (Fig. 1b). Vertical slip may start on all sides of the octogon, the RSS being equal, 0.213 P_0, but in the experiment $\{0\,0\,1\}_0$ was seen to appear first, while cross-slip occurred to $\{\bar{1}\,1\,1\}_0$ and $\{\bar{1}\,1\,0\}_0$. P_0 is the maximum pressure in the contact.

0022–2461/89 $03.00 + .12

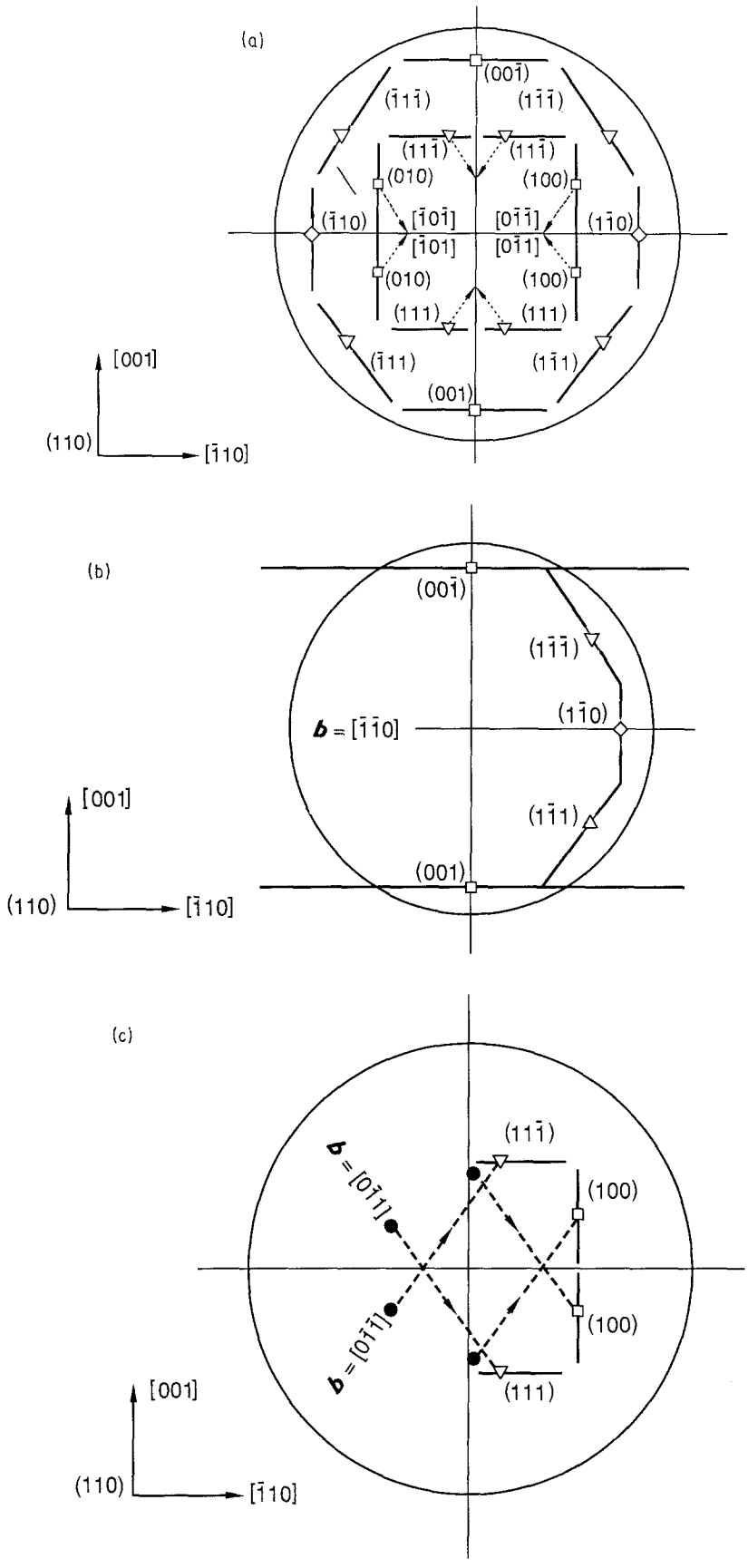

Figure 1 (a) Contact circle with slip lines expected for vertical slip (the outer octogon) and for inclined slip, with the Burgers vectors along the $\langle 1\,1\,0\rangle$ directions under 60° with the normal on the (1 1 0) surface. The radius of the circle, a, is of the order of 20 μm. The symbols (□ {1 0 0}, ▽ {1 1 1} and ◇ {1 1 0}) indicate the position where the Burgers vector is expected on the surface when it is drawn from the position of maximum RSS. (b) The outer pattern consists of eight lines, the right half of which is seen when sliding to the right. (c) The inner pattern consists of eight perpendicular lines, which may overlap. The Burgers vectors are under 60° with the normal on (1 1 0). The four lines shown form the pattern when sliding to the right.

The inner pattern is due to slip on two systems, {1 0 0} and {1 1 1}. Here slip may occur along any of inclined four Burgers vectors, each with its own pattern (Fig. 1c). If, for example, $\boldsymbol{b}$ is along [0 $\bar{1}$ $\bar{1}$], slip could start on $(1\,1\,\bar{1})_{60}$ with the larger RSS, 0.282 P_0. In the indentations more lines were seen first on $(1\,0\,0)_{60}$ with 0.256 P_0. Some of the lines were coupled to the $(1\,1\,\bar{1})_{60}$ lines, which suggested cross-slip between {1 0 0} and {1 1 1}. The other possible lines for this Burgers vector, due to $(1\,\bar{1}\,1)_{60}$ (RSS = 0.121 P_0) and $(0\,1\,\bar{1})_{60}$ (RSS = 0.210 P_0) were not observed after indentation.

The present work is concerned with the slip patterns observed after sliding on a (1 1 0) plane of the ferrite. The following questions were addressed. Firstly, is it possible to identify the slip patterns after sliding as well as after indenting, and does this allow a relation between the RSS and the strain in the groove?

Secondly, by varying the speed of sliding, is it possible to decide which process is the bottleneck in producing slip, nucleation or propagation? Thirdly, how does the ductile behaviour change when the temperature is raised? And finally, does the relative humidity affect the ductility as much as it does cracking?

2. Methods of investigation

2.1. Experimental details

Grooves were made as described previously [7, 13, 14, 15]. The grooves on the sample were observed after the experiment under a microscope equipped with Nomarski interference contrast. In most photos to be shown the light comes from the north-west. The dimensions of the grooves were measured by means of a profiler, scanning perpendicular to the scratching direction. Grooves with a depth of 10 to 500 nm could be measured in this way.

Crystals of manganese zinc ferrite, $Mn_{0.62}Zn_{0.32}Fe_{2.06}O_4$ were used, made by the Bridgman technique. Blocks were cut and the surface of the (1 1 0) face was diamond-polished. The c.l.a. roughness is 2 nm.

2.2. Calculations

The resolved shear stress (RSS) on a slip plane was calculated by Schmidt's formula using the stress distribution underneath a loaded sphere, as given by Hamilton [9, 10]. The elastic modulus in $Mn_{0.62}Zn_{0.32}Fe_{2.06}O_4$ varies from $E = 127$ GPa in the $\langle 0\,0\,1\rangle$ direction to 227 GPa for $\langle 1\,1\,1\rangle$ [16]. In $\langle 1\,1\,0\rangle$ the vertical modulus is 189 GPa, while the Poisson constant varies from 0.07 along $[\bar{1}\,1\,0]$ to 0.56 along [0 0 1]. In the calculation an effective value is needed, here the average value, 0.315, was used. The radius of the contact circle, a, and the maximum stress in the contact, P_0 are derived from the Hertz equations [17].

A problem is that Hamilton's equations are for isotropic materials, with a constant Poisson constant in all directions. In Mn–Zn ferrite there is a considerable variation. Chen [18] has used the full compliance tensor for a plane strain calculation. His method might be useful to estimate this effect. At present there is no readily available analytical expression for the stress in the general case.

3. Slip line patterns

3.1. Sliding along the $\langle -1\,1\,0\rangle$ direction

Grooves made along $[1\,\bar{1}\,0]$ under a load of 5 N show how the patterns change with speed (Fig. 2). The patterns will be analysed using Fig. 1. At 400 μm sec^{-1} the groove consists of two parallel lines, due to $(1\,1\,\bar{1})_{60}$ and $(1\,1\,1)_{60}$. At 40 μm sec^{-1} the perpendicular $(1\,0\,0)_{60}$ and $(0\,1\,0)_{60}$ lines are found, as well as the $(0\,0\,1)_0$ of the "outer" pattern. Note the black colour of the 60° lines, it indicates that a positive step is formed in front of the sphere. On decreasing the speed further new lines are added, $(\bar{1}\,1\,1)_0$ and $(\bar{1}\,1\,\bar{1})_0$ along 55° with the direction of sliding, and $(\bar{1}\,1\,0)_0$, vaguely visible in the centre (Fig. 2c). This photo was illuminated along the groove to enhance the visibility of the lines under 55°. This, however, makes the $(1\,1\,\bar{1})_{60}$ and $(1\,1\,1)_{60}$ lines invisible, although present on the surface. Some transverse lines due to $(0\,1\,0)_{60}$ are still present. At 0.4 μm sec^{-1}, the same lines were found. The end of the groove shows scratches that were absent at the start and were made during sliding (Fig. 2d). We note a tendency of the $(1\,1\,\bar{1})_{60}$ lines to move across the pattern made by the $(0\,0\,1)_0$ lines, an example is seen in Fig. 2b.

In a 7 N groove made at 400 μm sec^{-1} the pattern is again simple. The $(1\,1\,1)_{60}$ and the $(1\,1\,\bar{1})_{60}$ lines are seen, but, in contrast to the 5 N groove, now in the presence of $(0\,0\,1)_0$. At 40 μm sec^{-1} the $(\bar{1}\,1\,\bar{1})_0$ and $(\bar{1}\,1\,1)_0$ lines appear (Fig. 3a), while at lower speeds the $(\bar{1}\,1\,0)_0$ lines are visible, always connected to the $(\bar{1}\,1\,\bar{1})_0$ and $(\bar{1}\,1\,1)_0$ (0.4 μm sec^{-1}, Fig. 3b). At this load cracks are sometimes seen, shaped as horseshoe cracks.

For sliding along this direction, the evidence for cross-slip from $(1\,1\,1)_{60}$ to $(0\,1\,0)_{60}$ is not very clear. In 3.4. we return to this issue. The conditions under which the slip lines appear have been summarized in Table I.

3.2. Higher temperature

On increasing the temperature to 155 and 290° C, the grooves become more pronounced and more lines are present, even at low loads. For a single pass of 4 N along $[1\,\bar{1}\,0]$, made at 155° C with 4 μm sec^{-1}, the vertical system shows vague lines of $(\bar{1}\,1\,\bar{1})_0$ and $(\bar{1}\,1\,1)_0$, but more lines of $(\bar{1}\,1\,0)_0$ are visible. There are several $(0\,0\,1)_0$ lines along the groove's edge. The 60° system is present with the transverse $(0\,1\,0)_{60}$ and $(1\,0\,0)_{60}$ lines, while $(1\,1\,1)_{60}$ is not observed (Fig. 4a).

At 290° C, here shown at 4 N, single pass and 40 μm sec^{-1}, the $(1\,1\,1)_0$ and $(1\,1\,1)_{60}$ lines are absent (Fig. 4b). The $(1\,\bar{1}\,0)_0$ is clearly visible in the centre of the groove, as well as the $(0\,0\,1)_0$ and $(0\,0\,\bar{1})_0$ lines along the groove and the transverse lines due to $(1\,0\,0)_{60}$.

TABLE I Conditions of appearance of slip when sliding on the (1 1 0) surface along $[1\,\bar{1}\,0]$

		Conditions			Temperature	Dry/wet	Cross-slip
Load		4 N	5 N	7 N			
P_0 (GPa)		6.30	6.80	7.61			
a (μm)		17.4	18.7	21.0			
System	RSS/P_0	Max. speed at 20° C					
$(1\,1\,\bar{1})_{60}$	0.28	40	400–4	400–4	low	dry	no
$(0\,1\,0)_{60}$	0.26	4	40	400	all	always	no
$(0\,0\,1)_0$	0.21	4	40	400	all	always	no
$(\bar{1}\,1\,1)_0$	0.21	0.4	4	40	low	dry	yes
$(\bar{1}\,1\,0)_0$	0.21	–	0.4	4	high	dry	yes/no

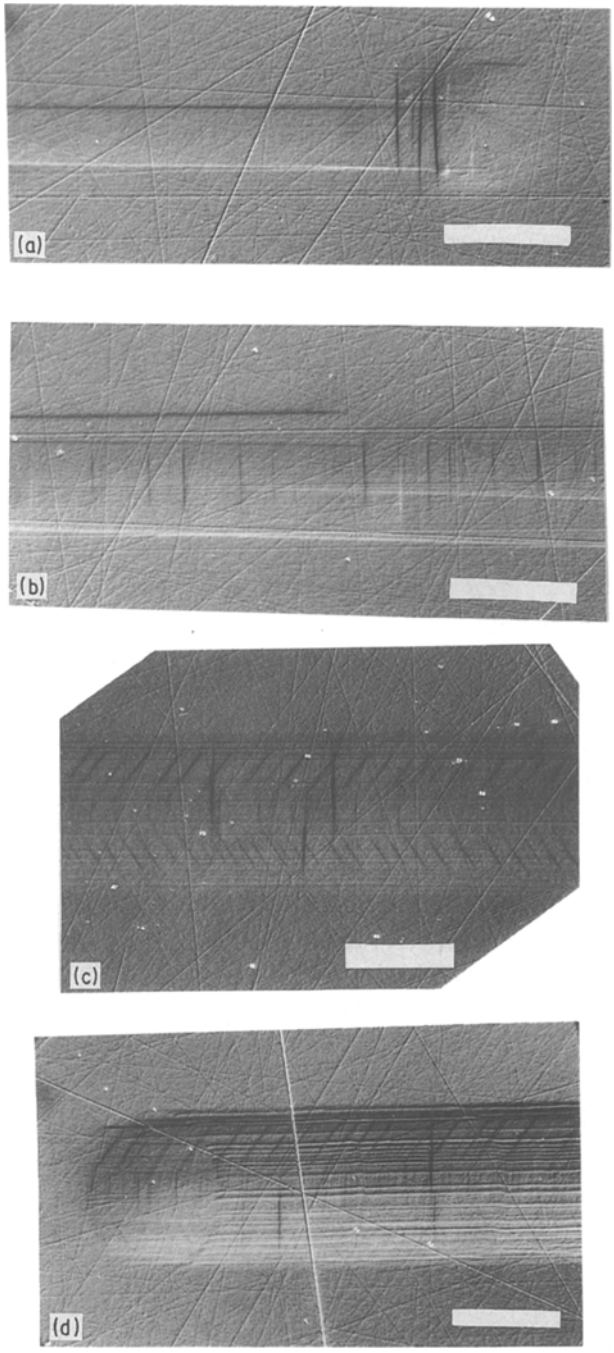

Figure 2 Grooves made at a load of 5 N, one pass to the left at various speeds. Scale bar = 30 μm. (a) At 400 μm sec^{-1} the lines due to $(1\,1\,\bar{1})_{60}$ and $(1\,1\,1)_{60}$ are seen. At the start the indentation is visible, where the vertical $(0\,1\,0)_{60}$ and the horizontal $(0\,0\,\bar{1})_0$ are visible. (b) At 40 μm sec^{-1} the lines due to $(1\,0\,0)_{60}$ are now clearly present. (c) At 4 μm sec^{-1} the $\{1\,1\,1\}$ lines on the vertical system are present, the $\{1\,1\,0\}$ lines on the same system are vaguely visible in the centre. In this case the illumination is not at an angle, but straight down the groove. (d) At 0.4 μm sec^{-1}, the end of a groove shows fine scratches due to debris taken along by the sphere. Groove depth 245 nm. Slip on the three vertical systems is now very clear, but, as in indentations the $\{1\,1\,1\}$ system for the inclined slip is overruled. The $(0\,1\,0)_{60}$ lines transverse to the groove are still visible.

Repeating passes and lower speeds produce cracks more often than at 20° C. Scratches and smearing effects make the observation of the lines more difficult.

In conclusion, at the higher temperatures the cross-slip to $\{1\,1\,1\}_0$ disappears, while the $\{0\,0\,1\}_0$ and $\{1\,1\,0\}_0$ are both present. The $\{1\,1\,0\}_0$ lines are no longer connected to the $\{1\,1\,1\}_0$'s, moreover they are as

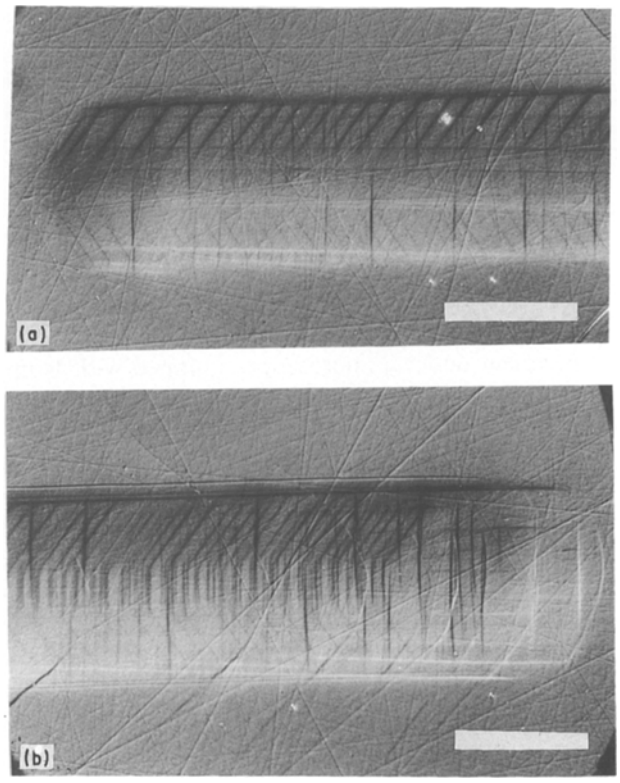

Figure 3 Groove patterns, made at 7 N load, single pass to the left at various speeds. Scale bar = 30 μm. (a) At 40 μm sec^{-1}, at the end of the groove, all of the lines of the indentation (Fig. 1) are seen, except the $\{1\,1\,0\}$ lines in the centre. Cone cracks are present in some of the grooves. (b) At 0.4 μm sec^{-1} the start resembles the low load indentation, showing the $(1\,0\,0)_{60}$ lines, black in front, white when made behind the sphere. The horizontal lines due to $(1\,1\,1)_{60}$ are here visible, but disappear down the groove. The $\{1\,1\,0\}$ in the centre are clear, as well as the $\{1\,1\,1\}$ lines due to vertical slip. Depth 380 nm. Several cone cracks occur along the groove.

short as at 20° C, therefore nucleation must have occurred independently. The effect of the higher temperatures has been summarized in Table I.

3.3. Wet sliding

A few experiments were done at 3 N, single pass, at various speeds along $[\bar{1}\,1\,0]$. At 40 μm sec^{-1} no groove is present, at 4 μm sec^{-1} a small number of $(0\,1\,0)_{60}$ and $(1\,0\,0)_{60}$ lines are seen. At 0.4 μm sec^{-1} these lines are more abundantly present, together with the $(0\,0\,1)_0$ along the edges. Increasing the number of passes leads to more lines, but to heavy cracking as well (Fig. 5). It is interesting to note that the 55° lines due to $\{1\,1\,1\}_0$ are absent under these conditions. The results on the influence of humidity have been added to Table I.

3.4. Angular variation

The anisotropy of the occurrence of the slip patterns was investigated by varying the direction of sliding. A low load was used in order to simplify the analysis of the slip line patterns. At 4 N, 400 μm sec^{-1} for a single pass there is no groove at all, but with 10 passes in both directions simple patterns are made. In this case P_0 equals 6.3 GPa and the contact radius a is 17.4 μm. The groove depth, measured at three places along the groove, varies with the angle ϕ, taken from the $[\bar{1}\,1\,0]$ direction. The data for $\phi > 90°$ are combined with those for $180 - \phi$ (Fig. 6). Data on the Knoop

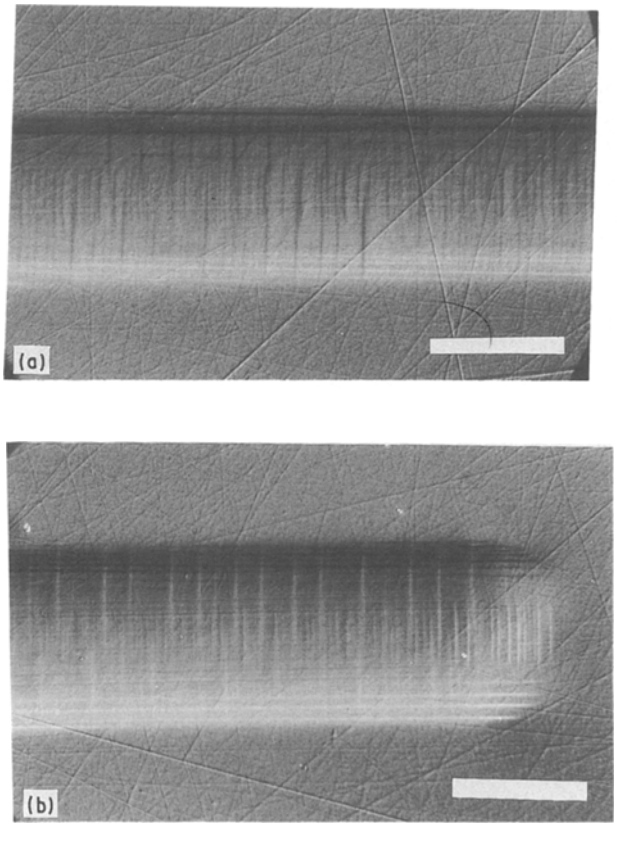

Figure 4 Patterns made at higher temperatures, at 4 N load, single pass. Scale bar = 30 μm. (a) At 155° C, 4 μm sec^{-1} to the left, showing the lines due to the vertical system, although the $(1\,1\,1)_0$ are vague. For the 60° system the lines due to $(1\,0\,0)_{60}$ are visible, those due to $(1\,1\,1)_{60}$ are not observed. (b) At 290° C and 40 μm sec^{-1} to the right, the end of the groove shows many lines due to $(1\,0\,0)_0$, $(1\,1\,0)_0$ and $(1\,0\,0)_{60}$, but no $(1\,1\,1)_0$ and $(1\,1\,1)_{60}$. Note the change in colour of the transverse lines, black when the sphere moves to the left (a), white in (b). In both cases the lines correspond to a positive step, made in front of the sphere.

hardness, taken at 3 N load, 30 sec [11], show the same angular variation as the groove depth (Table II).

Sliding along $[\bar{1}\,1\,0]$ the borders of the groove are formed by $(1\,1\,1)_{60}$ and $(1\,1\,\bar{1})_{60}$, as can be seen from the distance of 20 μm between the lines, which is clearly less than the width of the groove expected for the $(0\,0\,1)_0$ lines from the patterns at 5 N. Along the groove but at an angle of about 5°, lines due to $(1\,1\,\bar{1})_{60}$ and $(1\,1\,1)_{60}$ are seen, as well as some vertical lines of $(0\,1\,0)_{60}$ and $(1\,0\,0)_{60}$ (Fig. 7a). Sliding at an angle of 30° with $[\bar{1}\,1\,0]$ shows the $(1\,0\,0)_{60}$, $(0\,1\,0)_{60}$, $(1\,1\,1)_{60}$ and $(1\,1\,\bar{1})_{60}$ lines (Fig. 7b). The same pattern, but with different numbers of lines, is found for 30 to 80° and 100° to 150°, (120° is shown in Fig. 7c). The $\{1\,0\,0\}_{60}$ lines are clearly connected to the $\{1\,1\,1)_{60}$, indicating cross-slip. At 90°, sliding along [0 0 1], no $(1\,1\,1)_{60}$ and

TABLE II Sliding on (1 1 0). Angular variation of the number of slip lines per mm for two slip systems, A, $\{1\,1\,1\}_{60}$ and B, $\{1\,0\,0\}_{60}$, and the depth of groove for 4 N, 400 μm sec^{-1}

Angle direction	°0 $[\bar{1}\,1\,0]$	20°	40°	90° [0 0 1]
system A, lines (mm)	continuous	80	65	0
system B, lines (mm)	80	100	130	continuous
groove depth (nm)	128	152	133	172
H_k (GPa) [2]	5.73	5.78	5.73	6.28

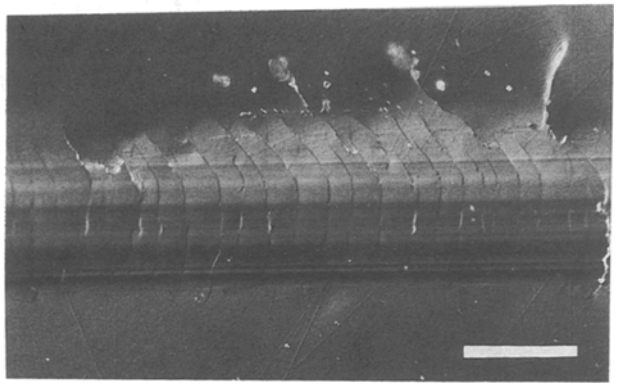

Figure 5 Pattern made at 20° C, 3 N, 40 μm sec^{-1} and 10 passes in both directions under water. Scale bar = 30 μm.

$(1\,1\,\bar{1})_{60}$ lines are present any more, while the $(1\,0\,0)_{60}$ and $(0\,1\,0)_{60}$ lines are continuous (Fig. 7d). The density of the two sets of lines is given in Table II.

The length of the lines depends on their orientation. The lines that are more in the direction of the groove are longer. The lines, more or less transverse to the groove, are interrupted before the groove's edge is reached, but reappear farther down the groove.

4. Discussion

4.1. Depth in relation to pattern

According to previous results [15] the groove depth, d, (nm) after sliding on (1 1 0) along $\langle\bar{1}\,1\,0\rangle$ at 20° C, increases with load and number of passes, N, and decreases with speed, v, according to

$$d = 74F_n + 101^{10} \log N - 58^{10} \log v - 148 \quad (1)$$

where the units of v are μm sec^{-1}. At higher temperatures the groove is deeper and occurs at lower loads than at 20° C, while under wet conditions the (1 1 0) grooves were not deeper than when dry.

The line patterns observed here show in general the same trend. The number of lines increases with F_n, passes, temperature and decrease with speed. In agreement with Equation 1 the patterns at a given combination of load and speed, resemble those at a lower load and lower speed (Table I). Not all lines, however, behave in the same way and a direct relation between number of slip lines and groove depth cannot be given.

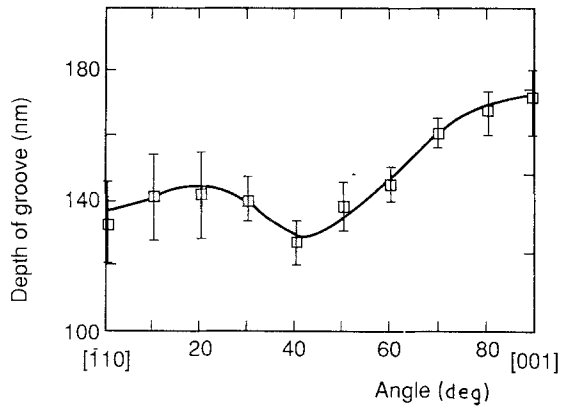

Figure 6 Depth plotted against direction of sliding in (1 1 0) at F_n = 4 N, v = 400 μm sec^{-1} and 10 passes (both ways).

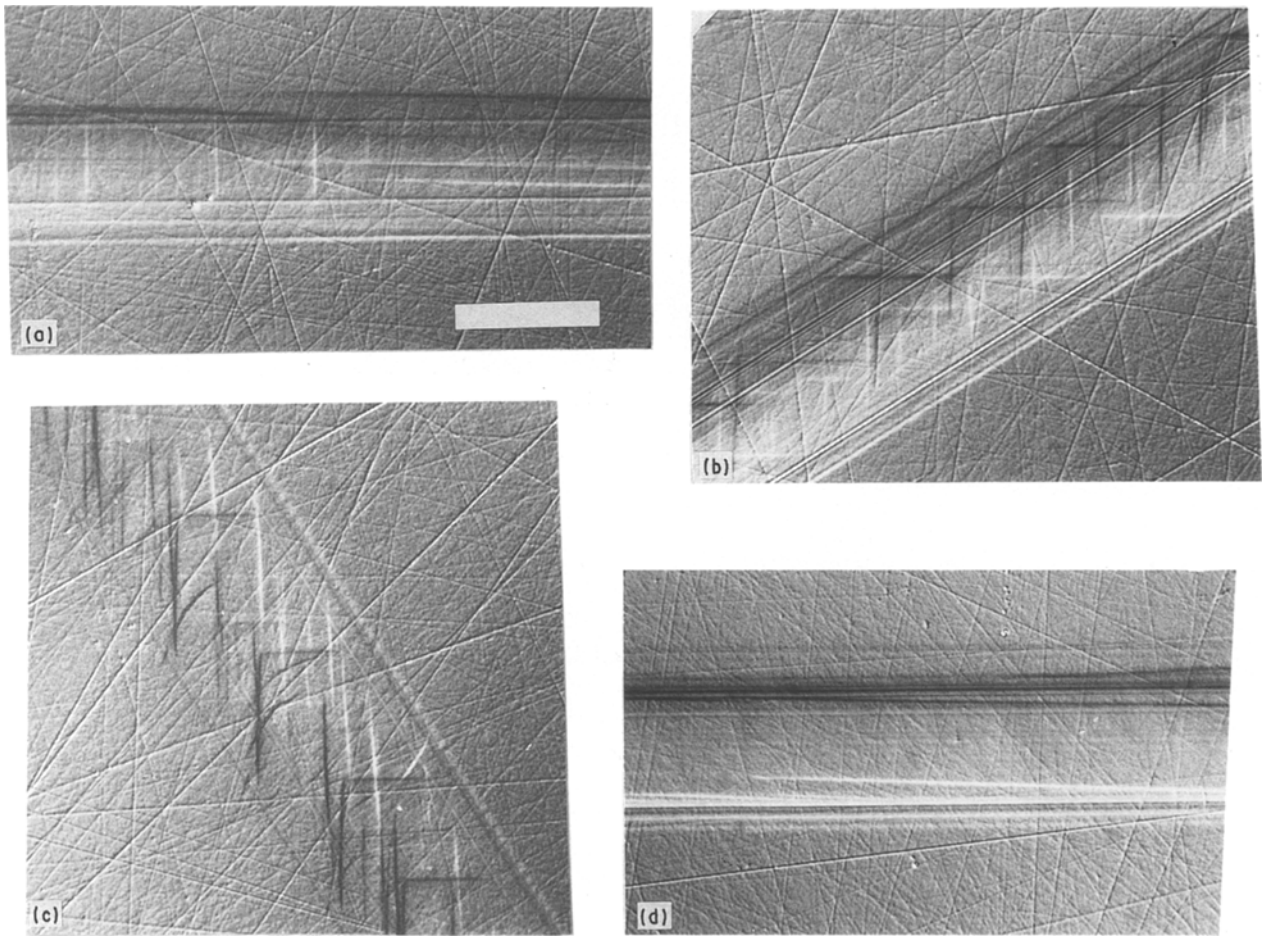

Figure 7 Groove patterns for 4 N load, 400 μm sec^{-1}, 10 passes both ways. Scale bar = 30 μm. (a) Pattern made along $\langle \bar{1}\,1\,0 \rangle$, showing lines due to $(1\,1\,1)_{60}$ and $(0\,1\,0)_{60}$. (b) Pattern for a groove made at 30° with $\langle 1\,\bar{1}\,0 \rangle$, both $(1\,1\,1)_{60}$ and $(0\,1\,0)_{60}$ are visible, coupled to each other in some places. (c) Groove at 120° C, (equivalent to 60°). Pattern as at 30°, but several cone cracks are seen. (d) Groove at 90°, showing only the $(0\,1\,0)_{60}$ lines, marking the boundaries of the groove.

A few examples are now given:

(i) While at higher load or lower speed the depth increases, there is a change in the pattern. Slip on the $\{1\,1\,1\}_{60}$ system disappears and is taken over by $\{1\,1\,1\}_0$ and $\{1\,1\,0\}_0$ in the center of the groove.

(ii) When sliding is done in water instead of dry, the $\{1\,1\,1\}_{60}$, $\{1\,1\,1\}_0$ and $\{1\,1\,0\}_0$ lines are no longer present, but the depth is not affected. However, a correlation between depth and number of remaining lines, $\{1\,0\,0\}_{60}$ and $\{0\,0\,1\}_0$, is still present, since both increase when sliding at lower speed.

(iii) When the temperature is raised the depth increases, although the $\{1\,1\,1\}_0$ are no longer observed. Other lines are present, $\{1\,1\,0\}_0$, $\{0\,0\,1\}_0$ and $\{1\,0\,0\}_{60}$. Here again, a higher speed decreases the number of lines, but in spite of the change in pattern, the relation between depth and speed is the same as at room temperature [15].

(iv) When the direction of sliding is changed, the number of $\{1\,1\,1\}_{60}$ and $\{1\,0\,0\}_{60}$ lines varies (Table II). Here the direction of sliding selects the slip systems that may propagate without interruption (being parallel to the groove), while slip on other planes must await a new event of nucleation (being transverse to the groove and therefore of finite length). The depth, however, is only slightly affected by the appearance and disappearance of the lines (Fig. 6).

Once a slip line is present, its length may depend on the conditions of the experiment. Here, as in indentations [7, 8], we have not observed that the dimensions of the pattern change with load or speed. We conclude that a slip line, once it is present, grows as far as the RSS allows. Subsurface blocking of slip does not seem to occur. This result implies that the speed dependence of the patterns must be due to a time effect in the nucleation process: if the RSS is available during too short a time, nucleation will not occur. At higher temperature nucleation becomes much easier, as seen in the higher density of the lines.

4.2. The primary and secondary systems

At low load and high speed, after one pass, the patterns are simple and may help in identifying the primary slip systems. At high load, more passes and low speed, the patterns are more complicated because of cross-slip. This allows the identification of the secondary slip systems.

As in indentations the $\{1\,0\,0\}$ and $\{1\,1\,1\}$ systems with the inclined Burgers vector appear first. This agrees with the higher RSS values for the 60° slip direction (see the values when friction is absent in Table I). There is a difference of 0.026 in RSS/P_0 between the two 60° systems, the $(\bar{1}\,1\,1)_{60}$ having 0.282 and $(0\,1\,0)_{60}$ 0.256. In the indentations the latter

system produced more lines, but here it is the direction of sliding that determines which system becomes visible. A further analysis is given in the next section.

The vertical slip on $\{0\,0\,1\}_0$ appears at a higher speed than $\{1\,1\,1\}_0$ or $\{1\,1\,0\}_0$, or at a lower load as in the indentation experiments, although the RSS values for the three systems are equal (Table I). Before slip becomes activated, the available RSS must overcome a certain threshold. At higher temperatures the thresholds are lower, but the decrease may differ. For $(0\,0\,1)_0$ and $(\bar{1}\,1\,0)_0$ the threshold must have become lower than for $(\bar{1}\,1\,1)_0$, since the latter are absent at 290° C. Creep measurements [4–6] show that $\{1\,1\,1\}$ is present above 900° C, hence between 300 and 900° C the $\{1\,1\,1\}$ system reappears.

The conclusion is that on the (1 1 0) plane at room temperature the slip systems that first occur are $\{1\,0\,0\}_{60}$ and $\{1\,1\,1\}_{60}$, while with some more effort the vertical systems $\{0\,0\,1\}_0$, $\{1\,1\,1\}_0$ and $\{1\,1\,0\}_0$ appear respectively. All systems, whether primary or secondary, are speed dependent, i.e. a certain lapse of time is needed before activation occurs.

While in several cases new lines appear at a higher load or a lower speed, there is an exception. At high loads the $\{1\,1\,1\}_{60}$ system is not visible in the midst of the lines due to slip on the vertical system. It is possible that the two systems hinder each other, the $\{1\,1\,1\}_0$ and $\{1\,1\,0\}_0$ slip forming periodic walls that prevent the other system from propagating. Simultaneous slip propagation could also be difficult for the four Burgers vectors of the 60° system, since penetration must occur here as well (Fig. 2c).

The slightly inclined lines due to $\{1\,1\,1\}_{60}$ in a groove bounded by the $\{1\,0\,0\}_0$ lines (Fig. 7) suggest that the slip is not exactly on its plane. The $\{1\,1\,1\}$ lines due to the two different Burgers vectors remain parallel, however, thereby excluding various mechanisms, such as cross-slip to $\{1\,0\,1\}_{60}$.

4.3. Cracks and scratches

Brittle behaviour has been found in several grooves, mainly at higher loads. When a certain number of passes is exceeded, the number of lines does not increase any more and cracks appear. Sliding in water or at higher temperatures shows that the patterns are based on fewer slip systems, while more cracks are present than under standard conditions. We conclude that brittleness is found when ductile deformation is limited.

In the grooves made at low speeds, scratches were found at the end (Fig. 2d), even after a single pass. The fine grooves inside the large one are thought to be caused by fine particles, clinging to the sphere. These particles grow steadily and eventually deteriorate the slip line patterns. When slip lines are formed, for example in front of the sphere outside the contact circle, or on the front side of the contact, the passing of the sphere may fracture the protruding lines and produce fine particles [19, 20]. These are found as debris alongside the groove after many passes [13]. The scratches inside the groove are thus thought to be evidence of a small scale wear process.

4.4. Anisotropy on (1 1 0)

4.4.1. Comparison with Knoop hardness

The angular variation of the depth made at a low load, 4 N, high speed, $400\,\mu m\,sec^{-1}$ and 10 passes, was between 128 and 172 nm, i.e. $\pm 17\%$ (Fig. 6). In the data on wear in video recording, taken at $12\,m\,sec^{-1}$ [1], the opposite trend is seen, for $\phi = 0°$ the wear rate is high, for $\phi = 35$, 55 and 90° an order of magnitude lower. The difference in speed and the number of passes may be too large for comparison with our data, or the wear process is not primarily determined by slip as observed here.

On (1 1 0) the Knoop hardness varies by $\pm 5\%$ when the direction of the long axis is varied [2]. It is remarkable that the Knoop hardness data show the same maxima as the depth (Table II). This points to a significant difference between the Knoop hardness and the anisotropy, deduced from spherical sliding. Several authors have noted that the Knoop hardness has some remarkable properties. It is independent of the plane of measurement, but it clearly depends on the direction of the long axis [2, 21, 22]. By using cubic materials with different slip systems Chin *et al.* [22] noted that the Knoop hardness is independent of the slip system. Boyarskaya found, within a series of materials with the rocksalt structure with $\{1\,1\,0\}\langle 1\,\bar{1}\,0\rangle$ slip, that the Knoop anisotropy changes sign [23]. In the same structure, for cubic carbides, another remarkable effect is that the same anisotropy may be found, although different slip systems are activated [24]. Sargent and Page [25] found large differences in the hardness derived from the length and the width of the Knoop indentation on (1 0 0) MgO. The largest width occurs when the long axis is along [1 0 0], the smallest when the axis is along [0 1 1]. The differences were attributed to extrinsic effects, such as piling-up of material on the sides and to elastic recovery. It is not known how this works out in the Knoop data [2].

A few remarks about this problem may be added. The Knoop indenter introduces an asymmetric stress, treated approximately by Brookes [26]. Moreover, as every pyramidal indenter, there is a stress singularity where the four planes meet. The approximations and the singularity can be avoided by using an ellipsoid, for which the stress distribution is known. An ellipsoid is preferred above a knife [23], because it could probably be made with a better controlled surface quality. Using ellipsoids, however, would have to defy Sargents remark [26], that "only faceted indenters can reveal any anisotropy". This is true for measurements of the lateral dimensions of the indentation. Indeed, for a sphere indentation the radius of the contact circle is not very interesting, but the depth is [13, 15] and so are the patterns inside the indent [7, 8]. Measurement of the depth of spherical indentations and grooves allow the observation of the onset of first slip. Together with the known stress distribution a more satisfactory analysis is possible. The Knoop indenter may be convenient, because a value is easily measured, but the comparison with the present data shows again that its use is not without problems.

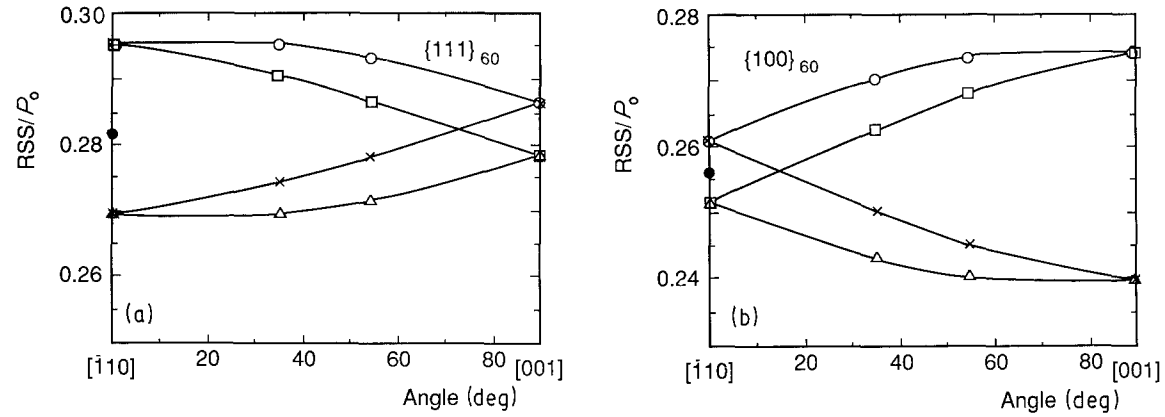

Figure 8 Influence of friction on the resolved shear stress, when the direction of the friction force is varied from $[\bar{1}\,1\,0]$ at $\phi = 0°$ to $[0\,0\,1]$ at $\phi = 90°$. (a) For the inclined slip systems (○) $(1\,1\,\bar{1})[\bar{1}\,0\,\bar{1}]$, (×) $(1\,1\,\bar{1})[0\,\bar{1}\,\bar{1}]$, (□) $(1\,1\,1)[\bar{1}\,0\,1]$, (△) $(1\,1\,1)[0\,\bar{1}\,1]$. For zero friction the RSS/P_0 value is 0.282. (b) For the inclined slip systems (○) $(1\,0\,0)[0\,\bar{1}\,\bar{1}]$, (×) $(1\,0\,0)[0\,\bar{1}\,\bar{1}]$, (□) $(0\,1\,0)$ $[\bar{1}\,0\,\bar{1}]$, (△) $(0\,1\,0)[\bar{1}\,0\,1]$. For zero friction the RSS/P_0 value is 0.256.

4.4.2. RSS calculations

In the experiment described in Section 3.4. the slip pattern is simple, only the slip system with the inclined Burger vector is activated. Two systems are involved, $\{1\,1\,1\}_{60}$ to be labelled "A", and $\{1\,0\,0\}_{60}$, "B", each with four slip directions, (see the centre of Fig. 1). The contribution of each of the slip systems can be understood by calculating the RSS on the slip planes for the four directions, taking into account that friction is present ($f = 0.1$), since the friction will change the RSS from the static value. For each combination of slip plane and slip direction the RSS shows an angular dependence (Fig. 8a, b). At the applied contact stress, P_0, in this experiment, slip occurs first for the system with the highest RSS. Therefore the two upper curves in each figure are relevant, whereas the slip systems of the lower curves are favoured when sliding in the opposite direction.

For zero friction RSS max equals 0.282 P_0 for system A, and 0.256 P_0 for system B. By introducing friction ($f = 0.1$) the highest RSS, 0.296 P_0, is found at $\phi = 0°$ for system A, see the upper two $\{1\,1\,1\}$ lines, (○) and (□) in Fig. 8a. At $\phi = 90°$ the (○) line has decreased to a lower value, 0.286 P_0. For the B system, the upper two $\{1\,0\,0\}$ lines, (○) and (□) in Fig. 8b, show the highest RSS, 0.274 P_0 at $\phi = 90°$, whereas at $\phi = 0°$ RSS is lower, 0.261 P_0. The two systems therefore act against each other, giving the possibility that one takes over from the other at a certain angle. The density of the lines observed show how this takes place (Table II). The RSS data can be used for estimating the influence of the number of passes Section 4.4.3. and for the yield curve of the two systems A and B Section 4.4.4.

4.4.3. Repeating passes

For a single pass, made at 400 μm sec^{-1} and $\phi = 0°$, no lines were observed at a load of 4 N, but at 5 N the first appeared (Fig. 2). The same pattern was found for 4 N when the number of passes was increased to 20, 10 in both directions (Fig. 7a). Since the RSS is calculated from the load, the effect of 20 passes is equivalent to a difference in load of 1 N. This of course is a rough estimate, yet it may be compared with the effect of 20 passes on the depth. From Equation 1 the load should be decreased by (101 log 20)/74 = 1.76 N to obtain the same depth. For system A, $\{1\,1\,1\}_{60}$, the effect of 20 passes is equivalent to an increase of RSS from 1.86 to 2.01 GPa, a difference of 0.15 GPa. For B, $\{1\,0\,0\}_{60}$, this is about the same, 0.13 GPa (Table III).

4.4.4. Depth–RSS curves

The angular variation of the depth (Fig. 6) can be combined with the RSS in the following analysis. The line pattern at $\phi = 0°$ shows a continuous line for $(1\,1\,\bar{1})$ $[\bar{1}\,0\,\bar{1}]$ (Fig. 7a). On increasing ϕ, these lines become shorter, until they disappear at $\phi = 70°$. The corresponding RSS values are found from the upper lines of Fig. 8a (the ○ symbols). The lines for the other A system, $(1\,1\,1)$ $[\bar{1}\,0\,1]$, are present at $\phi = 0°$ as well, but these disappear above about 35°, where RSS/P_0 equals 0.290. This is the same value as that where the other line stopped (Table III).

The same analysis can be made for the other system,

TABLE III RSS values for the $\{1\,1\,1\}_{60}$ and $\{1\,0\,0\}_{60}$ systems at 400 μm sec^{-1}

Conditions		A, $\{1\,1\,1\}_{60}$				B, $\{1\,0\,0\}_{60}$			
Load	Passes	Angle	RSS/(P_0)	RSS (GPa)	Pattern	Angle	RSS/P_0	RSS (GPa)	Pattern
4 N	$N = 1$	0	0.296	1.86	no lines	90	0.274	1.73	no lines
5 N	$N = 1$	0	0.296	2.01	lines	90	0.274	1.86	lines
4 N	$N = 20$	0	0.296	1.86	lines	90	0.274	1.73	lines
4 N	$N = 20$	$\geqslant 70$	0.291	$\leqslant 1.83$	no A1	0	0.262	1.65	B1
		> 35	0.290	$\leqslant 1.83$	no A2	$\leqslant 30$	0.262	$\geqslant 1.65$	B2

A1 = $(1\,1\,\bar{1})[\bar{1}\,0\,\bar{1}]$ B1 = $(1\,0\,0)[0\,\bar{1}\,\bar{1}]$
A2 = $(1\,1\,1)[\bar{1}\,0\,1]$ B2 = $(0\,1\,0)[\bar{1}\,0\,\bar{1}]$

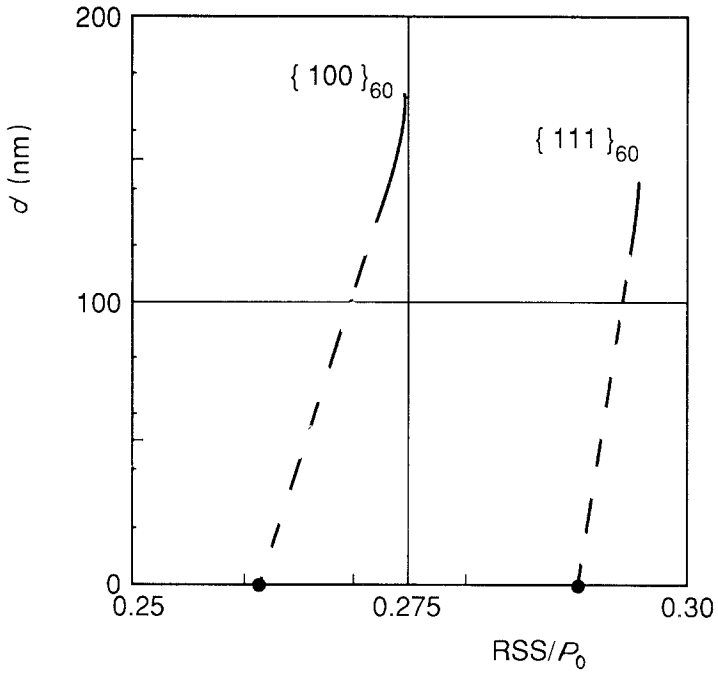

Figure 9 Depth (equivalent to strain) plotted against RSS/P_0 for the two slip systems that are active at low load, $\{1\,1\,1\}_{60}$ and $\{1\,0\,0\}_{60}$. The full lines indicate the stress range where these systems are active, the interrupted lines connect to the threshold where the lines disappear.

$\{1\,0\,0\}$, at $\phi = 90°$. One of the lines, due to $(1\,0\,0)$ $[0\,\bar{1}\,\bar{1}]$, remains visible over the whole range to $\phi = 0°$, where it shows up as a transverse line (Fig. 7a). The slip lines corresponding to the second curve in Fig. 8b (the □ symbols), are present from $\phi = 90°$ to $\phi = 30°$. In terms of RSS this means that the □ line disappears at RSS/P_0 = 0.262. The same value is found for the other line of this system (Table III).

Over the range from $\phi = 0°$ to $\phi = 90°$ the lines of the A system dominate at low angles, while above, say, 45°, the B lines are more abundant. If we assume that the depth is due to the dominating system, a depth-resolved shear stress curve may be constructed. The curves for 20 passes and $v = 400\,\mu m\,sec^{-1}$ are shown for the two systems in Fig. 9. The RSS/P_0 value where slip stops, was derived in Section 4.4.2 and is shown by a black dot. For the A system the difference between the start (1.86 GPa) and stop (1.83 GPa) values of RSS is rather small, less than for the B system with 1.73 and 1.65 GPa (Table III). For a lower number of passes or a higher speed all values are expected to be higher. The RSS where slip stops is in the range found in indentations, for $\{1\,1\,1\}$ at 0.9 to 1.8 GPa, for $\{1\,0\,0\}$ 0.6 to 1.65 GPa [8].

5. Conclusions

A model experiment has been described where a sliding sphere provides information on the plastic deformation of a ferrite crystal. Calculations of the resolved shear stress have been used in reaching the following conclusions.

(1) The slip line patterns in the groove consist of polygons as in indentations. Primary and secondary systems can be distinguished. The patterns from all slip systems are speed dependent.

(2) At low loads, the pattern is due to slip on $\{1\,1\,1\}$ and $\{1\,0\,0\}$ with Burgers vectors under 60°. By varying the direction of sliding the two slip systems are seen to change in intensity. Over a wide range of angles the lines are connected by cross-slip.

(3) The angular variation of the groove depth is similar to that of the Knoop hardness, instead of being the inverse.

(4) From the data on the depth and the calculated resolved shear stress it is possible to construct a yield curve for the 60° systems.

(5) At higher load or lower speed a different pattern appears, due to slip on three planes, $\{1\,0\,0\}$, $\{1\,1\,1\}$ and $\{1\,1\,0\}$, with a vertical Burgers vector. At still higher load it dominates the $\{1\,1\,1\}$ pattern due to the inclined system. Cross-slip occurs from $\{0\,0\,1\}$ to $\{1\,1\,1\}$ and from here to $\{1\,1\,0\}$. Cross-slip is interrupted along the groove.

(6) At higher temperatures less cross-slip is observed, the vertical and the inclined $\{1\,0\,0\}$ systems are present and short lines of $\{1\,1\,0\}$, as an independent system. Evidence for thermally stimulated propagation has not been found and nucleation seems to form the bottleneck for the patterns.

(7) At room temperature in a water droplet the groove appears at the same load, but only the $\{1\,0\,0\}$ systems are observed. Cracking occurs at much lower loads than when sliding dry.

References

1. K. KUGIMIYA, E. HIROTA and N. ITO, *IEEE Trans. Mag.* **MAG-10** (1974) 907–909.
2. T. ITO, *J. Amer. Ceram. Soc.* **54** (1971) 24–26.
3. K. MIYOSHI and D. H. BUCKLEY, *Wear* **66** (1981) 157–173.
4. M. UEMURA, T. HYONO, M. UMENO and H. KAWABE, *J. Mater. Sci.* **21** (1986) 2257–2263.
5. T. NISHIKAWA, Y. OKAMOTO and N. OKADA, *J. Soc. Mat. Sci. Jpn* **30** (1981) 337, 1012–1018.
6. S. L. CALLAHAN, R. E. TRESSLER, D. W. JOHNSON and M. J. REECE, "Slip systems in Manganese Zinc Ferrite Crystals, Deformation in ceramic materials II", edited by R. E. Tressler and R. C. Bradt (Plenum, New York, 1983) pp. 177–186.
7. A. BROESE VAN GROENOU and S. E. KADIJK, *Acta Metall.* **37** (1989) in press.
8. S. E. KADIJK and A. BROESE VAN GROENOU, *ibid.* **37** (1989) in press.

9. G. M. HAMILTON and L. E. GOODMAN, *J. Appl. Mech.* **33** (1966) 371–376.
10. G. M. HAMILTON, *Proc. Inst. Mech, Eng.* **197C** (1983) 53–59. (The equation for σ_x due to a tangential load contains a term $x^2z^2/3$; 3 should be S.)
11. M. V. SWAIN, *Wear* **48** (1978) 173–180.
12. M. V. SWAIN and B. R. LAWN, *Phys. Status Solidi* **35** (1969) 909–923.
13. A. BROESE VAN GROENOU and S. E. KADIJK, *Wear* **126** (1988) 91–110.
14. N. MAAN and A. BROESE VAN GROENOU, *ibid.* **42** (1977) 365–390.
15. A. BROESE VAN GROENOU and S. E. KADIJK, *Wear.* **131** (1989) 353–364.
16. G. DE WITH and J. P. M. DAMEN, *J. Mater. Sci.* **16** (1981) 838.
17. S. P. TIMOSHENKO and J. N. GOODIER, "Theory of Elasticity" 3rd edn (McGraw-Hill, New York, 1970).
18. W. T. CHEN, *Int. J. Solids Structures* **5** (1969) 191–214.
19. D. KUHLMANN-WILSDORF, in "Fundamentals of Friction and Wear of Materials", edited by D. A. Rigney (American Society for Metals, Metals Park, Ohio, 1980) pp. 119–186.
20. Y. J. CHANG and D. KUHLMANN-WILSDORF, in Proceedings International Conference on Wear of Materials, Reston, VA, April 11–14, 1983, edited by K. C. Ludema (American Society of Mechanical Engineers, New York, 1983) pp. 414–425.
21. M. GARFINKLE and R. G. GARLICK, *Trans. Metall. Soc. ASME* **242** (1968) 809–814.
22. G. Y. CHIN, M. L. GREEN, L. G. VAN UITERT and W. A. HARGREAVES, *J. Mater. Sci.* **8** (1973) 1421–1425.
23. Y. S. BOYARSKAYA, D. Z. GRABKO and E. I. PURICH, *ibid.* **14** (1979) 737–741.
24. R. H. J. HANNINK, D. L. KOHLSTEDT and M. J. MURRAY, *Proc. R. Soc.* **A326** (1972) 409–420.
25. P. M. SARGENT and T. F. PAGE, *J. Mater. Sci.*. **20** (1985) 2388–2398.
26. C. A. BROOKES, J. B. O'NEILL and B. A. W. REDFERN, *Proc. R. Soc.* **A322** (1971) 73–88.

Received 13 October 1988
and accepted 20 January 1989